2021 43rd Annual International Conference of the
IEEE Engineering in Medicine & Biology Society (EMBC)
Oct 31 - Nov 4, 2021. Virtual Conference

The Paradigm Design of a Novel 2-class Unilateral Upper Limb Motor Imagery Tasks and its EEG Signal Classification

Wenzheng Qiu[1], Banghua Yang[1,*], Jun Ma[1], Shouwei Gao[1], Yan Zhu[2], Wen Wang[3,*]

Abstract—**Multitasking motor imagery (MI) of the unilateral upper limb is potentially more valuable in stroke rehabilitation than the current conventional MI in both hands. In this paper, a novel experimental paradigm was designed to imagine two motions of unilateral upper limb, which is hand gripping and releasing, and elbow reciprocating left and right. During this experiment, the electroencephalogram (EEG) signals were collected from 10 subjects. The time and frequency domains of the EEG signals were analyzed and visualized, indicating the presence of different Event-Related Desynchronization (ERD) or Event-Related Synchronization (ERS) for the two tasks. Then the two tasks were classified through three different EEG decoding methods, in which the optimized convolutional neural network (CNN) based on FBCNet achieved an average accuracy of 67.8%, obtaining a good recognition result. This work not only can advance the studies of MI decoding of unilateral upper limb, but also can provide a basis for better upper limb stroke rehabilitation in MI-BCI.**

I. Introduction

Motor Imagery based Brain Computer Interface (MI-BCI) is one of the three important paradigms of Brain Computer Interface (BCI) [1]. The principle of MI-BCI is that during motor imagery (MI) or motor execution, the localized neural rhythmic activity in the contralateral motor-sensory areas of the cerebral cortex is significantly diminished, while in the ipsilateral motor-sensory areas increases, most significantly in the μ-rhythm (8-12 Hz) and β-rhythm (18-25 Hz), known as Event-Related Desynchronization (ERD) or Event-Related Synchronization (ERS) [2]. With the progress of BCI research, the application areas of MI-BCI become more extensive, such as upper limb exoskeleton control [3] and stroke rehabilitation [4].

In stroke rehabilitation domain, MI-BCI has unique advantages in activating the plastic potential of neuronal cells in specific regions of the brain through active imagery form of rehabilitation to achieve reconstruction or repair of control functions between limb and brain, which can promote faster recovery of stroke patients [4]. MI-BCI currently focuses on both left and right hands, mainly because the cerebral location of ERD/ERS is on different sides of the brain when performing left- and right-handed MI, which is distinguished more easily than that of unilateral [5]. Consequently, there are fewer studies on multitasking MI-BCI of the same upper limb [6]. However, stroke patients usually have unilateral limb paralysis, and they could enhance the motor function of paralyzed limbs through the rehabilitation of multiple motions of the affected limb, so the study of unilateral limb multitasking MI-BCI has a better realistic value for stroke rehabilitation [7].

Studies targeting unilateral upper limb multitasking MI-BCI have received attention and some progress has been made. For example, Yong et al. [8] first proposed the MI-BCI classification of two motions of the unilateral upper limb, while Chu et al. [9] proposed the MI-BCI classification of three different parts of the upper limb, separately obtaining 60.6% and 66.2% accuracy. Current studies, however, in addition to the insufficient number of subjects, unspecific MI motions have brought challenges in practical application in stroke rehabilitation.

In this paper, Section II designed two novel unilateral upper limb MI tasks, hand gripping and releasing (hand-grasping) and elbow reciprocating left and right (arm-reaching) for stroke patients to meet the rehabilitation needs. Section IIIA visualizes the EEG signal of MI from time and frequency domains to verify the presence of ERD and ERS like conventional left- and right-handed MI tasks. Section IIIB introduces three EEG recognition methods, common spatial pattern (CSP) [10], filter bank common spatial pattern (FBCSP) [11] and the optimized convolutional neural network (CNN) based on FBCNet [12]. Among them, the CSP method, which filters the original EEG signal in the spatial domain and extracts discriminative features, and the FBCSP method, which applies CSP to different sub-bands and combines features with different frequency domain information, both of them using SVM Classifier [10], are baseline methods widely used in MI-BCI decoding and recognized to have good results, and CNN-based methods can rapidly improve the recognition accuracy of MI-BCI, similar to EEGNet [13] and deep and shallow ConvNets [14], achieving higher accuracy than baseline methods. Section IV shows the classification results the methods above, and then these accuracies statistically analyzed to find the similarities and differences with the previous left- and right-handed MI tasks.

II. Materials

A. Experimental Paradigm

Ten healthy right-handed healthy subjects (five males and five females, 22-30 years old) participated in this experiment.

This research work is supported by National Natural Science Foundation of China (No. 61976133), Major scientific and technological innovation projects of Shan Dong Province (2019JZZY021010), Shanghai Industrial Collaborative Technology Innovation Project (2021-cyxt1-kj14).

[1]Wenzheng Qiu, Banghua Yang, Jun Ma and Shouwei Gao are with School of Mechatronic Engineering and Automation, Research Center of Brain Computer Engineering, Shanghai University, Shanghai, 200444, China. Email: yangbanghua@shu.edu.cn

[2]Yan Zhu is with Department of Neurological Rehabilitation, The Second Rehabilitation Hospital of Shanghai, Shanghai, 200441, China.

[3]Wen Wang is with Department of Radiology & Functional and Molecular Imaging Key Lab of Shaanxi Province, Tangdu Hospital, Fourth Military Medical University, Xi'an, Shaanxi, 710038, China. Email: wangwen@fmmu.edu.cn

Wenzheng Qiu is the first author.

Banghua Yang and Wen Wang are corresponding authors.

None of them had experience in MI-BCI. The experimental procedures involving human subjects described in this paper were followed the Helsinki Declaration. The timeline of each trial of the paradigm in this experiment is shown in Fig. 1.

Each trial lasts 7.5s, of which the first 1.5s are video and audio cues for the two designed motions of right hand. These two detailed MI tasks were developed based on the difficulty and efficiency of rehabilitation, after communicating with clinicians in several hospitals. The details of the motions are shown in Fig. 2, where the specific MI in Fig. 2(a) is multiple reciprocal gripping and releasing of the unilateral hand, and in Fig. 2(b) is multiple reciprocal left-right movements of the unilateral elbow. Then MI tasks indicated on the screen for 4s, with the progress bar presented to tip elapsed time and no unnecessary visual and auditory stimuli. Lastly, a black screen is shown for 2s with a voice prompt of break.

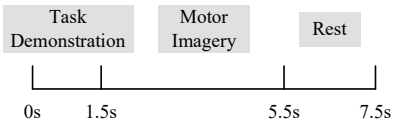

Figure 1 Timing of one trial of our experimental paradigm.

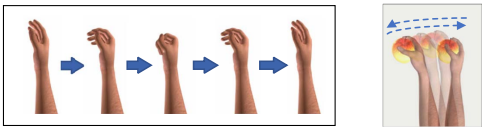

(a) (b)

Figure 2 Two motions of our motor imagery task, including hand gripping and releasing (a), and elbow reciprocating left and right (b).

Before the experiment started, a resting state with eyes open and eyes closed, each lasting 1 minute. The experiment consisted of 5 sessions, each consisting of 40 trials, with 20 trials for each MI task, and a 1-minute rest between sessions. Thus, 200 trials of data can be collected from one subject in one experiment.

B. Data Collection and Preprocessing

The acquisition equipment for this experiment was CGX Quick-30 Dry EEG Headset according to the standard 10/20 System, with specific 30 channels shown in Table 1.

TABLE I. ALL CHANNELS OF THE EEG HEADSET.

Number	1	2	3	4	5	6	7	8
Channel	Fp1	Fp2	AF3	AF4	F7	F8	F3	Fz
Number	9	10	11	12	13	14	15	16
Channel	F4	FC5	FC6	T7	T8	C3	Cz	C4
Number	17	18	19	20	21	22	23	24
Channel	CP5	CP6	P7	P8	P3	Pz	P4	PO7
Number	25	26	27	28	29	30		
Channel	PO8	PO3	PO4	O1	O2	A2		

Electrode impedances were kept within 100kΩ during the whole experiment, and the frequency was 1000Hz. The EEG cap used a bandpass filter of 0.1Hz-100Hz by default settings of the headset. The data were downsampled to 250Hz for reducing computational cost during data processing. The preprocessing of the acquired data was done with the EEGLAB toolbox (v2019.1) [15] of MATLAB (R2020a) software.

III. METHODS

A. Analysis of ERDS During MI

During two novel upper limb MI tasks, pronounced ERD/RES patterns emerged, and raw EEG data will be used to analyze the ERD pattern in both the time and frequency domains. In order to make the presented results more intuitive, one certain subject (S04) was selected in this part, and the EEG signals were firstly divided into two categories according to different MI tasks. Secondly the average electric potential value and power spectrum density of all 100 trials of each category of the C3 electrode were calculated. Finally, the differences between the two sets of signals were analyzed.

In time domain, the EEG signal was first band-pass filtered in mu band (8-12Hz) in preprocessing, after which the C3 channel was selected and its time series of two MI tasks were obtained according to the average value calculation process. Fig. 3(a) shows the comparison of electric potential changes with time for electrode C3, where two motions showed different decreasing curves with time, which is consistent with ERD pattern in the left parietal lobe of the brain region.

In frequency domain, the EEG signal was first band-pass filtered in available band (1-40Hz) in preprocessing, after which the same process as the average value calculation. Fig. 3(b) shows the comparison of power spectral density (PSD) changes with frequency for electrode C3, where two motions showed ERD pattern around the mu (8-12Hz) and beta (18-25Hz) bands for the two MI tasks. Around these two frequency bands, a large difference in PSD between two motions, indicates that the two motions activate different levels of motor areas of the brain.

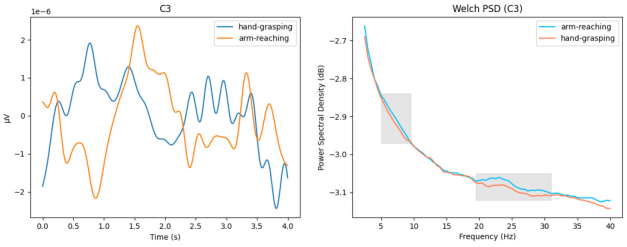

(a) (b)

Figure 3 The comparison of electric potential changes with time (a) and power changes with frequency (b) during two motor imagery tasks for electrode C3 in the Subject S04.

B. CSP Method and Its Pattern Analysis

The first decoding method used is Common Spatial Pattern (CSP) [10], primarily based on detecting the patterns of ERDS. CSP is a spatially filtered feature extraction method for two classification tasks, aimed to extracting the spatially components of each class from raw EEG data. The principle is to use the diagonalization of the matrix to find an optimal set of spatial filters for projection, obtaining a feature vector discriminating 2 classes of EEG signals by maximizing the variance. The specific principle and implementation of CSP is described in [10].

To confirm whether the features extracted using CSP method for new MI tasks can be effectively classified, the feature vectors of the patterns of CSP spatial filter generated for each subject are visualized in the form of a brain

topography map to visualize the differences between features. Fig. 4 shows the first and last CSP patterns for 10 subjects. It can be seen a significant difference between CSP0 and CSP1 for each subject, which proves that the features extracted by each subject under CSP method are well discriminated.

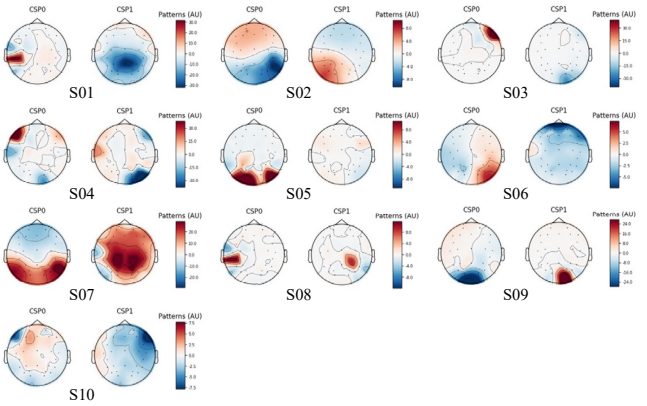

Figure 4 The topographic patterns of first two components of CSP of total 10 subjects in the experiment.

C. FBCSP Method and Its Pattern Analysis

Filter Bank Common Spatial Pattern (FBCSP) [11] method is based on CSP method with improvements in frequency filtering and feature selection. A filter bank is used to divide EEG signal in multiple sub bands to extract different features, which is set as 4-40Hz, with every 4Hz divided into one sub-band, such as 9 bands of 4-8Hz, 8-12Hz, ..., 36-40Hz. The specific principle and implementation process FBCSP is described in [11].

Similar to the pattern analysis of the CSP, the feature vectors of the 9 sub bands of the FBCSP, are presented in the brain topography. Fig. 5 shows FBCSP patterns of 4-40Hz in one certain subject (S09), where it can be found that the features of each sub-band are different, and the contrast around beta band, such as 20-24Hz, are more obvious, proving that the method is also effective in extracting MI features for different motions of unilateral upper limb. More importantly, this discrimination provides a basis for band selection of FBCSP and even other methods.

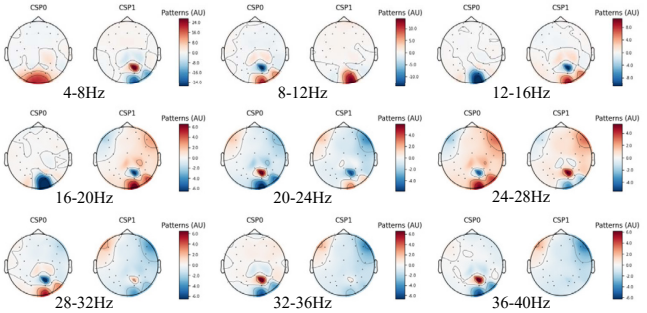

Figure 5 The topographic patterns of first two components of FBCSP of total 9 sub-bands of the Subject S09 in the experiment.

D. Optimized CNN based on FBCNet

FBCNet [12] is a novel deep learning algorithm that combines neurophysiological priors and Convolutional Neural Network (CNN) for MI-BCI classification by extracting spectro-spatial discriminative features in few learning parameters, while avoiding overfitting problem in case of small datasets. In this paper, a network is constructed on the basis of FBCNet, whose structure is shown in Fig. 6. Same as FBCSP, the EEG signal is band-pass filtered through a filter bank. It contains a spatial CNN layer to learn discriminative spatial patterns, a unique variance layer that computes the variance of the signal power in time domain, and a fully connected layer for classifying MI tasks with the features extracted from the variance layer.

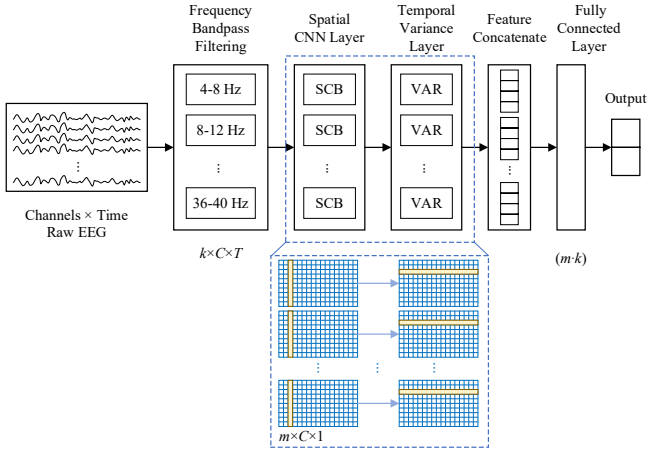

Figure 6 Architecture of optimized CNN based on FBCNet.

The spatial convolutional layer consists of N_b=k (In this paper k=9) parallel Spatial Convolution Blocks (SCB), each SCB module including 3 parts, a spatial convolutional module with a 2-dimensional convolution layer (Conv2d) of m spatial filters of size (C, 1) with C channels, a batch-normalization layer (BatchNorm2d), and an Exponential Linear Unit (ELU) activation function. The k SCB correspond to the number of sub bands filtered results as input, and the dimension of the output of SCB is m×T×k, with T sampling points. The output will be passed to the variance layer, and the variance on time domain of each time series is calculated using (1) in forward pass.

$$x^{VL}_{i,-,k} = \frac{1}{T}\sum_{j=1}^{T}\left(x^{SCB}_{i,j,k} - \mu_{i,-,k}\right)^2 \tag{1}$$

In this paper, the network structure is optimized based on FBCNet. The number of m is set as 4 to simplify the network structure and reduce the training time. In addition, the related early stop and training reset strategies are also established, as shown in Fig. 7.

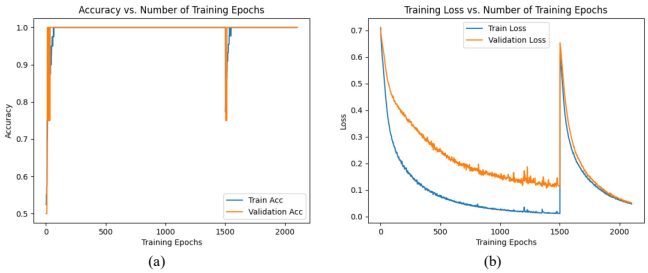

(a) (b)

Figure 7 The accuracy (a) and loss (b) with training epochs of CNN, taking one of 10 folds of the Subject S07 as an example.

Fig. 7 shows the training process of the network in detail, taking the training and validation accuracy (Fig. 7(a)) and loss

(Fig. 7(b)) of one certain subject's (S07's) 10-fold cross validation in one fold as an example. Before the training reset, the accuracy of the training and validation sets soar to almost 1, while their losses continue to fall throughout the period. Furthermore, the accuracy and loss repeat the above process after reset, while the loss decreases more rapidly. Eventually, the loss of the validation set reaches a much lower value than before, demonstrating the effectiveness of the strategy.

IV. Results

For the EEG data from 10 subjects, multiple algorithms were used to compare the accuracy of individual models between each subject. To fully simulate the flow of a real-time MI-BCI rehabilitation system for stroke patients (Training, model generating and testing), the performance comparison took the same data division approach, whereby each subject was divided into two equal parts chronologically, and the first half used 10-fold cross-validation to screen the optimal model, and the second half was tested to obtain the accuracy. Table 2 shows the comparison of the average accuracies using 3 methods in Section III, and Fig. 8 shows the accuracy of each subject in 3 methods sorted by the results of CSP algorithm.

TABLE II. Comparison of Average Classification Accuracy.

Method	Accuracy (%)
CSP+SVM	62.8 ± 12.12
FBCSP+SVM	64.0 ± 12.58
CNN based on FBCNet	67.8 ± 14.19

As can be seen in Fig. 8, firstly, for the four subjects on the lower end of the distribution (<60% accuracy) in CSP algorithm, both FBCSP and CNN achieved much higher results, with deep learning framework bringing great advantages. Secondly, for the subjects on the middle of the distribution (60-80% accuracy), the accuracy of FBCSP was comparable to that of CSP, while the accuracy of CNN would rise to a high level. Finally, for two subjects on the higher end of the distribution (>80% accuracy), the performance of FBCSP and CNN will be lower than that of CSP, but still remain at a good level.

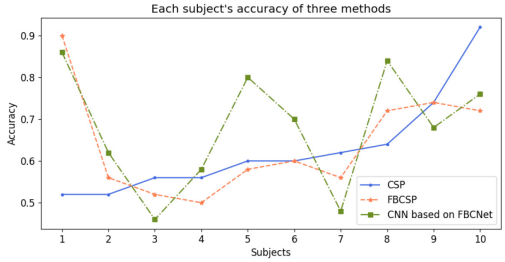

Figure 8 Average accuracy in the binary classification of two MI tasks using 10-fold cross-validation. (Sorted by CSP-SVM acc.).

It suggests that the result of distribution is consistent with conventional MI classification, such as BCI competition IV dataset 2a [11] and Korea University dataset [16], which can be illustrated that the two novel upper limb MI tasks are statistically distinguishable in terms of their distribution, and can be followed up the studies of post-stroke rehabilitation for upper limbs in MI-BCI.

V. Conclusion

In this paper, a novel MI-BCI experimental paradigm to acquire EEG data of 2-class unilateral upper limb of 10 normal people was designed. Three algorithms were applied, the highest of which achieved 67.8% classification results. It points out that MI tasks of unilateral upper limb could be accurately classified, and this work is informative for stroke rehabilitation in MI-BCI.

References

[1] J. J. Shih, D. J. Krusienski, and J. R. Wolpaw, "Brain-computer interfaces in medicine," in *Mayo Clinic Proceedings*, 2012, vol. 87, no. 3: Elsevier, pp. 268-279.

[2] A. A. Frolov, D. a. Húsek, E. V. Biryukova, P. D. Bobrov, O. A. Mokienko, and A. Alexandrov, "Principles of motor recovery in post-stroke patients using hand exoskeleton controlled by the brain-computer interface based on motor imagery," *Neural Network World,* vol. 27, no. 1, p. 107, 2017.

[3] A. Frisoli *et al.*, "A new gaze-BCI-driven control of an upper limb exoskeleton for rehabilitation in real-world tasks," *IEEE Transactions on Systems, Man, and Cybernetics, Part C (Applications and Reviews),* vol. 42, no. 6, pp. 1169-1179, 2012.

[4] K. K. Ang *et al.*, "A randomized controlled trial of EEG-based motor imagery brain-computer interface robotic rehabilitation for stroke," *Clinical EEG and neuroscience,* vol. 46, no. 4, pp. 310-320, 2015.

[5] E. B. Plow, P. Arora, M. A. Pline, M. T. Binenstock, and J. R. Carey, "Within-limb somatotopy in primary motor cortex–revealed using fMRI," *Cortex,* vol. 46, no. 3, pp. 310-321, 2010.

[6] B. J. Edelman, B. Baxter, and B. He, "EEG source imaging enhances the decoding of complex right-hand motor imagery tasks," *IEEE Transactions on Biomedical Engineering,* vol. 63, no. 1, pp. 4-14, 2015.

[7] A. A. Frolov *et al.*, "Post-stroke rehabilitation training with a motor-imagery-based brain-computer interface (BCI)-controlled hand exoskeleton: a randomized controlled multicenter trial," *Frontiers in neuroscience,* vol. 11, p. 400, 2017.

[8] X. Yong and C. Menon, "EEG classification of different imaginary movements within the same limb," *PloS one,* vol. 10, no. 4, p. e0121896, 2015.

[9] Y. Chu *et al.*, "Decoding multiclass motor imagery EEG from the same upper limb by combining Riemannian geometry features and partial least squares regression," *Journal of Neural Engineering,* vol. 17, no. 4, p. 046029, 2020.

[10] H. Ramoser, J. Muller-Gerking, and G. Pfurtscheller, "Optimal spatial filtering of single trial EEG during imagined hand movement," *IEEE transactions on rehabilitation engineering,* vol. 8, no. 4, pp. 441-446, 2000.

[11] K. K. Ang, Z. Y. Chin, H. Zhang, and C. Guan, "Filter bank common spatial pattern (FBCSP) in brain-computer interface," in *2008 IEEE International Joint Conference on Neural Networks (IEEE World Congress on Computational Intelligence)*, 2008: IEEE, pp. 2390-2397.

[12] R. Mane, N. Robinson, A. Vinod, S.-W. Lee, and C. Guan, "A Multi-view CNN with Novel Variance Layer for Motor Imagery Brain Computer Interface," in *2020 42nd Annual International Conference of the IEEE Engineering in Medicine & Biology Society (EMBC)*, 2020: IEEE, pp. 2950-2953.

[13] V. J. Lawhern, A. J. Solon, N. R. Waytowich, S. M. Gordon, C. P. Hung, and B. J. Lance, "EEGNet: a compact convolutional neural network for EEG-based brain–computer interfaces," *Journal of neural engineering,* vol. 15, no. 5, p. 056013, 2018.

[14] R. T. Schirrmeister *et al.*, "Deep learning with convolutional neural networks for EEG decoding and visualization," *Human brain mapping,* vol. 38, no. 11, pp. 5391-5420, 2017.

[15] A. Delorme and S. Makeig, "EEGLAB: an open source toolbox for analysis of single-trial EEG dynamics including independent component analysis," *Journal of neuroscience methods,* vol. 134, no. 1, pp. 9-21, 2004.

[16] M.-H. Lee *et al.*, "EEG dataset and OpenBMI toolbox for three BCI paradigms: an investigation into BCI illiteracy," *GigaScience,* vol. 8, no. 5, p. giz002, 2019.